(Received 26 March 2024, Accepted 19 May 2024, Scheduled 31 May 2024)

A Topology Reconstruction Based WPT System with CC and CV Outputs Function

Xuebin Zhou[1*], Yonghong Tan[1], Linhui Wang[1], and Lin Yang[2]

[1] College of Intelligent Manufacturing, Hunan University of Science and Engineering, Yongzhou, China
[2] College of Electronic and Electrical Engineering, Henan Normal University, Xinxiang, China

ABSTRACT: Constant current (CC) charging and constant voltage (CV) charging are the two main charging stages of lithium-ion batteries in wireless charging systems. The traditional LCC-LCC topology has a high degree of design freedom. The conversion from CC to CV output is usually achieved through composite topology or frequency switching, which results in high control complexity and increases system cost. This paper proposes a wireless power transfer (WPT) system with CC and CV output characteristics based on topology reconstruction. Based on the LCC-LCC topology, by introducing one MOSFET in the rectifier and one AC switch which consists of two MOSFETs connected in reverse series to reconfigure the topology, the conversion from CC to CV mode can be achieved without complicated control methods and additional components. In addition, the proposed system works at a fixed operating frequency point, which can effectively avoid frequency bifurcation phenomenon. Therefore, the proposed system features a simple structure, easy control, low cost, and high robustness. In addition, ZPA operation can be realized in both CC and CV modes, ensuring high transmission efficiency. An experimental prototype with a rated power of 480 W is built, and a maximum efficiency can reach 93.5%, which verifies the feasibility of the system.

1. INTRODUCTION

Wireless power transfer (WPT) system is an emerging technology, which provides energy for the load through magnetic coupling and realizes physical and electrical isolation [1–5]. Compared with the traditional plug-in charging, it has the advantages of convenience, safety, and flexibility, and has been used in many application fields, such as biomedical products [6, 7], electric vehicles [8–10], unmanned aerial vehicles [11–13], and other industrial areas [14, 15]. In recent years, high-performance lithium-ion batteries have been widely used in various applications. Fig. 1 shows the typical charging curve of a lithium-ion battery, which includes two main processes: constant current (CC) charging and constant voltage (CV) charging [16]. Charging starts in CC mode, and the battery voltage gradually increases during CC charging. When the battery voltage reaches the preset threshold, it switches to CV mode. Throughout the charging process, the battery equivalent resistance gradually increases.

To achieve CC and CV outputs, the common closed-loop control strategies applied in WPT system can be summarized as follows: phase modulation [17, 18], frequency control [19, 20], and DC-DC converter [21, 22].

Phase modulation technology ensures the CC or CV output when the load changes by adjusting the phase shift angle of the inverter or rectifier. However, the large duty change makes zero voltage switching (ZVS) difficult to achieve. Another approach is frequency control, which achieves CC or CV output characteristics by adjusting the operating frequency. However, this method forces the WPT system to face a large reactive power circulation, thereby greatly reducing the system efficiency. In addition, frequency splitting may also occur, resulting in reduced system stability. The above problems can be avoided by installing a DC-DC converter on the transmitter or receiver to adjust the output current or voltage, but the additional converter increases the weight, volume, and cost of the WPT system.

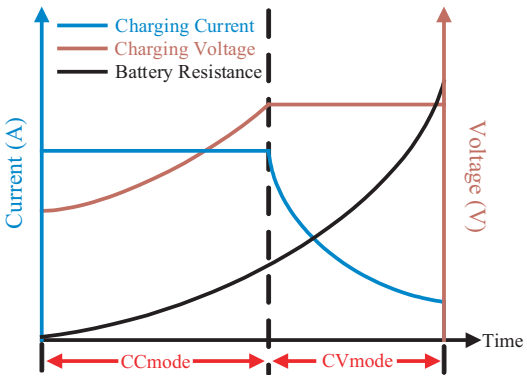

FIGURE 1. Typical charging curve of lithium battery.

Hybrid topology switching is a popular method at present. Compensations are normally employed in WPT systems to improve efficiency and achieve target characteristics. At resonant frequencies, S-S and LCC-LCC topologies have CC output function, while LCC-S and S-LCC have CV output characteristic [23]. By combining CC topology and CV topology, the load independent CC and CV dual output functions can be achieved, which is the basic principle of the hybrid topology switching

* Corresponding author: Xuebin Zhou (zhouxuebin821025@huse.edu.cn).

method [24–26]. However, this method requires excess compensation components and AC switches, which increases system development costs. Frequency switching method is another option worth choosing. For a specific topology, through reasonable parameter design, the system can achieve CC and CV charging outputs at two fixed frequency points respectively [27–30]. However, this method makes the system parameter design more complex, and the frequency change span is large, making it difficult to meet the standard requirements for frequency operation.

Considering the problems existing in the above methods, a WPT system based on topology reconfiguration is proposed in this study. The system only needs to control the working state of AC switch S and Metal-Oxide-Semiconductor Field Effect Transistor (MOSFET) Q_5 to realize the conversion between LCC-LCC topology and LCC-S topology without introducing excessive components and complex control strategies. This solution simplifies the circuit, reduces the control difficulty, saves the manufacturing cost of the system, and has certain practical value for battery pack charging applications.

The structure of this paper is as follows. In Section 2, the CC and CV characteristics are analyzed in detail. Section 3 gives the detailed parameter design process as well as simulated and experimental results. Finally, conclusions are drawn in Section 4.

2. THEORETICAL ANALYSIS

The architecture diagram of the proposed system is shown in Fig. 2. A full-bridge high-frequency inverter composed of Q_1, Q_2, Q_3, and Q_4 in the blue block diagram is used to invert the DC input voltage E and output it to the AC fundamental voltage U_i. L_P and L_S are the self-inductances of the transmitting and receiving coils, respectively. C_P and C_S are their respective compensation capacitors. L_1, C_1, L_2, and C_2 are the resonant components of the transmitting side and receiving side compensation topology, respectively. S is an AC switch, used to assist the system in converting between CC and CV modes. Q_5, D_1, D_3, and D_4 constitute the rectifier part of system. C_F is the filter capacitor; R_B is the battery load; R_P and R_S are the parasitic resistances of L_P and L_S, respectively. However, since parasitic resistance accounts for a small proportion of the overall loss, for the convenience of analysis, the influence of parasitic resistance is not considered in the analysis.

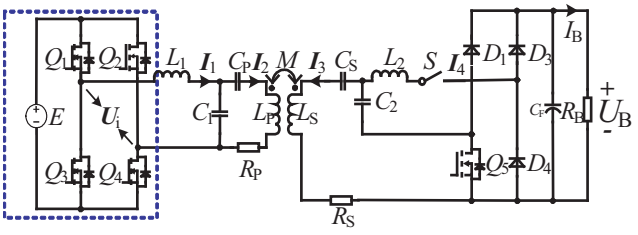

FIGURE 2. Architecture diagram of the proposed system.

According to [28], the input DC voltage source E and the root mean square (RMS) value of the inverter output AC voltage U_i satisfy Equation (1):

$$U_i = \frac{2\sqrt{2}E}{\pi} \tag{1}$$

I_B and U_B represent the charging current and voltage of the proposed system, which satisfies Equation (2).

$$\begin{cases} I_B = (\frac{\sqrt{2}}{\pi})I_4 \\ U_B = \frac{\pi}{\sqrt{2}}U_O \end{cases} \tag{2}$$

The resonance condition of the system is set to:

$$\begin{cases} \omega^2 L_1 C_1 = 1, \quad \omega^2 L_S C = 1 \\ \omega^2 L_2 C_2 = 1 \\ \omega^2 (L_P - L_1) C_P = 1 \\ \omega^2 (L_S - L_2) C_S = 1 \end{cases} \tag{3}$$

In Equation (3), capacitor C is the equivalent capacitance of capacitors C_S and C_2, and their equivalent relationship is:

$$C = \frac{C_S C_2}{C_S + C_2} \tag{4}$$

2.1. CC Mode

Figure 3 shows the overall structure diagram and equivalent circuit diagram of the proposed system in CC mode. When the system works in CC mode, the AC switch S and power MOSFET Q_5 are in the on state, and the system is equivalent to the LCC-LCC topology. Simultaneously, Diode D_3 and D_4 together form a half-bridge rectifier. R_E is the equivalent AC resistance, and its relationship with battery equivalent resistance R_B is:

$$R_E = \frac{2R_B}{\pi^2} \tag{5}$$

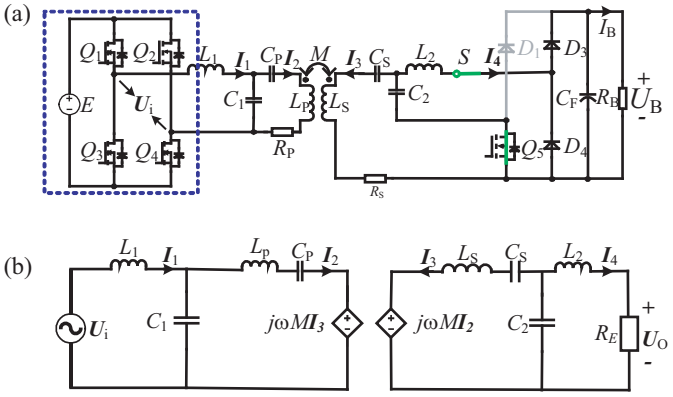

FIGURE 3. Overall structure diagram and equivalent circuit diagram of the proposed system in CC mode. (a) Overall structure diagram. (b) Equivalent circuit diagram.

According to Kirchhoff's voltage law (KVL), the following equation can be formulated for Fig. 3(b):

$$\begin{cases} (j\omega L_1 + \frac{1}{j\omega C_1})I_1 - \frac{1}{j\omega C_1}I_2 = U_i \\ -\frac{1}{j\omega C_1}I_1 + (\frac{1}{j\omega C_P} + \frac{1}{j\omega C_1} + j\omega L_P)I_2 + j\omega M I_3 = 0 \\ j\omega M I_2 + (\frac{1}{j\omega C_S} + \frac{1}{j\omega C_2} + j\omega L_S)I_3 + \frac{1}{j\omega C_2}I_4 = 0 \\ \frac{1}{j\omega C_2}I_3 + (\frac{1}{j\omega C_2} + j\omega L_2 + R_E)I_4 = 0 \end{cases} \tag{6}$$

Substituting Equation (3) into (6), Equation (7) can be deduced as

$$\begin{cases} I_1 = \frac{M^2 U_i R_E}{\omega^2 L_1^2 L_2^2} \\ I_4 = \frac{M U_i}{j\omega L_1 L_2} \end{cases} \tag{7}$$

Further, the expression of transconductance gain and input impedance can be obtained as

$$\begin{cases} G_{ui} = \frac{I_4}{U_i} = \frac{M}{j\omega L_1 L_2} \\ Z_{in} = \frac{U_i}{I_1} = \frac{\omega^2 L_1^2 L_2^2}{M^2 R_E} \end{cases} \tag{8}$$

Combining Equations (1), (2), and (8), the expression of charging current I_B can be obtained as

$$I_B = \frac{4}{\pi^2}\frac{ME}{\omega L_1 L_2} \tag{9}$$

Observing Equations (8) and (9), the charging current is not affected by the load change, and the input impedance is resistive, which means that the system can achieve CC output and zero phase angle (ZPA) operation.

2.2. CV Mode

In CC charging mode, when the charging voltage reaches the set threshold voltage, the AC switch S and MOSFET Q_5 will receive the control signal to perform a disconnection operation, thereby transitioning the system from LCC-LCC CC topology to LCC-S CV system. MOSFET Q_5 can be equivalent to a parasitic diode when being turned off. Subsequently, this parasitic diode and diode D_1 can form a half-bridge rectifier. Fig. 4 shows the overall structure diagram and equivalent circuit diagram of the proposed system in CV mode.

According to KVL, Equation (10) can be obtained.

$$\begin{cases} (\frac{1}{j\omega C_1} + j\omega L_1)I_1 - \frac{1}{j\omega C_1}I_2 = U_i \\ -\frac{1}{j\omega C_1}I_1 + (\frac{1}{j\omega C_1} + \frac{1}{j\omega C_P} + j\omega L_P)I_2 + j\omega M I_3 = 0 \\ j\omega M I_2 + (\frac{1}{j\omega C} + j\omega L_S + R_E)I_3 = 0 \end{cases} \tag{10}$$

Substituting Equation (2) into Equation (10), Equation (11) can be derived as

$$\begin{cases} I_1 = \frac{M^2 U_i}{L_1^2 R_E} \\ I_4 = \frac{M U_i}{L_1 R_E} \end{cases} \tag{11}$$

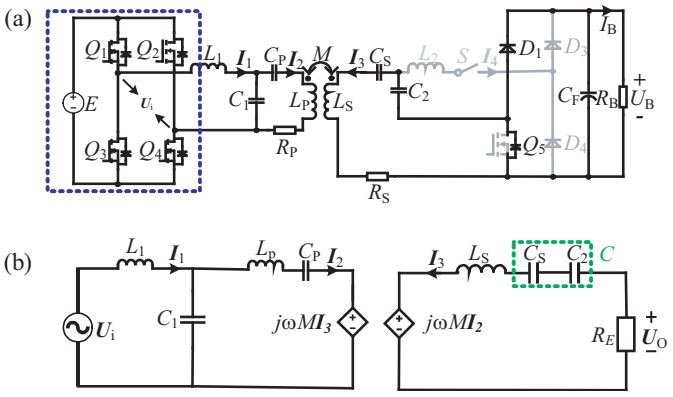

FIGURE 4. Overall structure diagram and equivalent circuit diagram of the proposed system in CV mode. (a) Overall structure diagram. (b) Equivalent circuit diagram.

Then, the expression of voltage gain and input impedance can be deduced as

$$\begin{cases} G_{uu} = \frac{U_o}{U_i} = \frac{M}{L_1} \\ Z_{in} = \frac{U_i}{I_1} = \frac{L_1^2 R_E}{M^2} \end{cases} \tag{12}$$

Combining Equations (1), (2), and (12), the expression of charging voltage U_B can be derived as

$$U_B = \frac{2ME}{L_1} \tag{13}$$

Observing Equations (12) and (13), the output voltage U_B is not affected by the battery load, and the input impedance exhibits purely resistive characteristics, which means that the system can achieve CV output and ZPA operation.

3. SIMULATION AND EXPERIMENTATION

3.1. Parameter Design

This paper carries a test example with a rated power of 480 W to verify the accuracy of the proposed system. Set its operating frequency to 100 kHz and the input DC voltage to 50 V. The charging current I_B and charging voltage U_B of the battery load are set to 4 A and 120 V, respectively. The detailed parameter design process of the proposed system is shown in Fig. 5.

Firstly, confirm the charging current I_B and charging voltage U_B according to the actual charging requirements. Then, the structure and size of the magnetic coupler are determined, and the corresponding self-inductance and mutual inductance are measured. Furthermore, the transconductance gain G_{ui} and voltage gain G_{uu} of the system are calculated to determine whether they meet the requirements. Finally, the parameters of compensation elements are calculated based on Equations (3), (9), and (13). The detailed parameters of the proposed system are listed in Table 1.

3.2. Simulation

According to the circuit parameters of the above design, the CC and CV characteristics of the proposed system and its ZPA op-

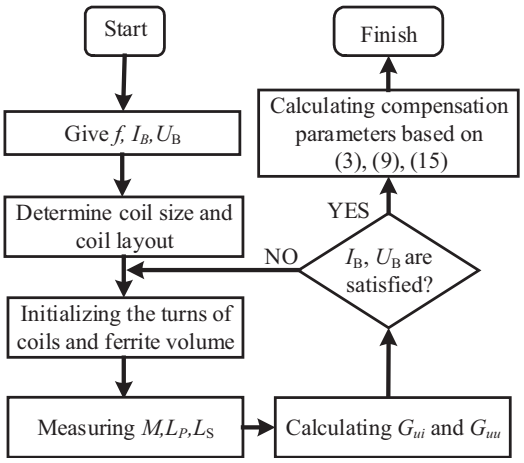

FIGURE 5. Parameter design process of the proposed system.

TABLE 1. The detailed parameters of the proposed system.

Parameter	Value	Parameter	Value
L_P	100 μH	L_S	100 μH
C_P	31.25 nF	C_S	27.78 nF
R_P	0.12 Ω	R_S	0.12 Ω
f	100 kHz	M	25 μH
L_1	20 μH	L_2	10 μH
C_1	125 nF	C_2	250 nF

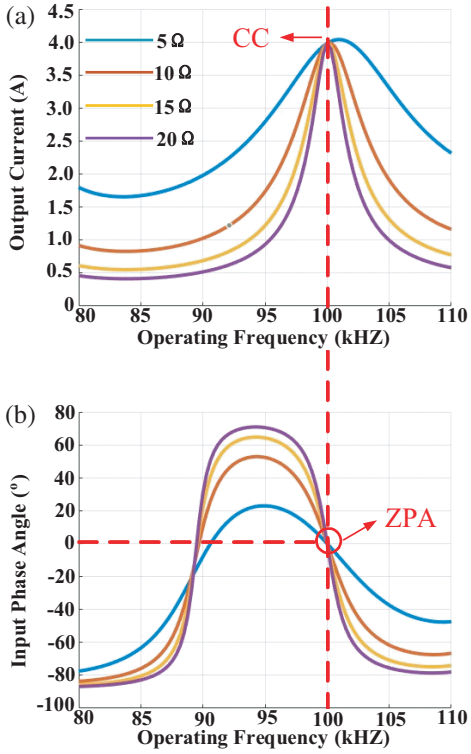

FIGURE 6. Verification of the CC and ZPA operation.

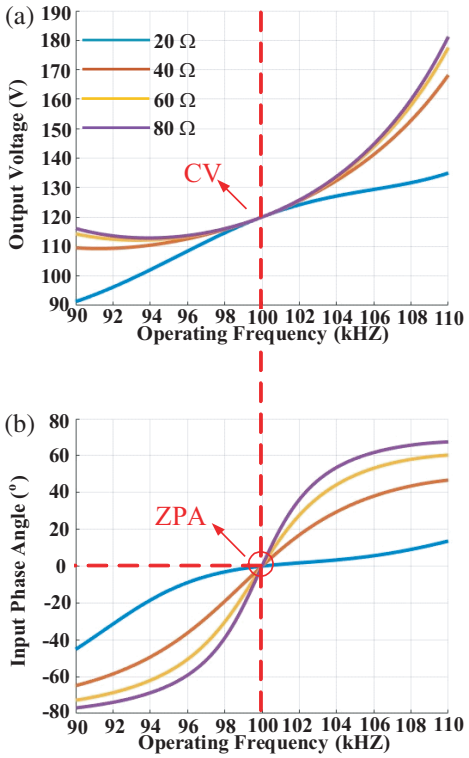

FIGURE 7. Verification of the CV and ZPA operation.

eration can be verified through the simulation software MATLAB. In CC mode, the load changes from 5 Ω to 20 Ω, and the output current I_B and input impedance angle change curves with frequency are shown in Fig. 6. It can be seen from Fig. 6 that when the load changes, both CC characteristic and ZPA operation can be achieved at the set frequency of 100 kHz. In CV mode, the load changes from 20 Ω to 80 Ω, and the output voltage and input impedance angle change curves with frequency are shown in Fig. 7. It can be seen from Fig. 7 that both CV characteristic and ZPA operation can be achieved at the set frequency of 100 kHz.

3.3. Experimental Verification

A confirmatory experimental setup with charging current of 4 A in CC mode and charging voltage of 120 V in CV mode is built, as shown in Fig. 8.

For CC output, the experimental waveforms when the load resistance is 5 Ω and 10 Ω are shown in Fig. 9. It can be observed from Fig. 9 that the charging current can be stabilized at 4 A under different load conditions. For CV output, the experimental waveforms when the load resistance is 50 Ω and 100 Ω are presented in Fig. 10. As evident in Fig. 10, the charging voltage can be stabilized at 120 V under different load conditions. The input current I_1 and input voltage U_i are basically in phase in both CC and CV modes, which means that ZPA operation is achieved.

Figure 11 displays the transient waveforms when the load resistance suddenly changes in both CC and CV modes. From Figs. 11(a) and (b), when the load resistance suddenly changes, the charging current I_B in CC mode and charging voltage U_B in

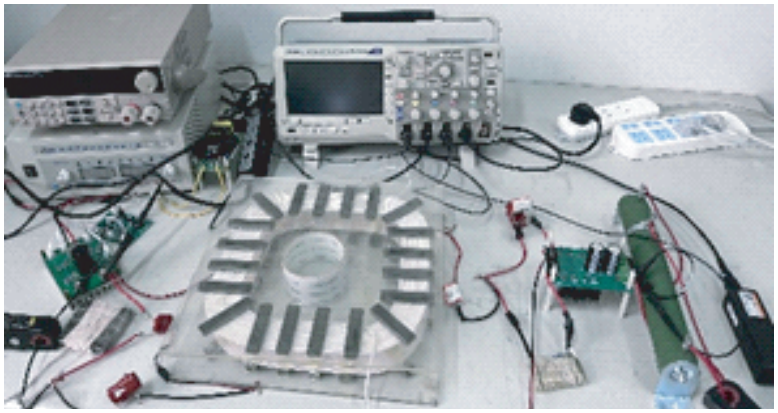

FIGURE 8. Experimental setup.

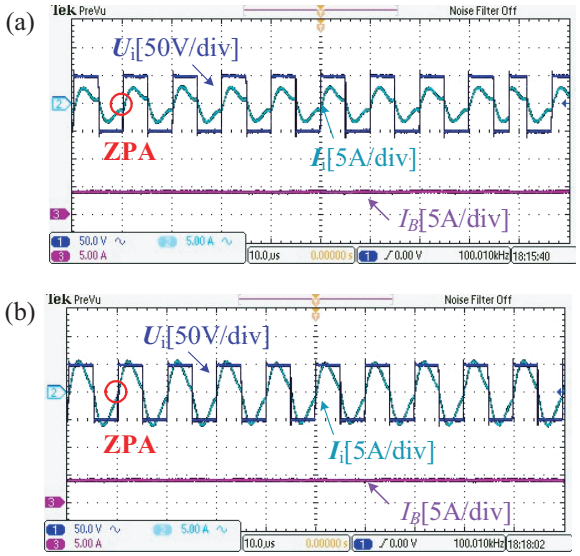

FIGURE 9. Experimental waveforms in CC mode. (a) $R_B = 5\,\Omega$ and (b) $R_B = 10\,\Omega$.

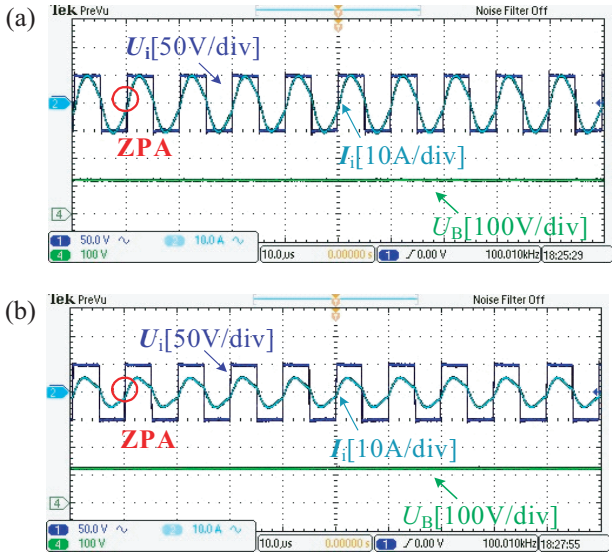

FIGURE 10. Experimental waveforms in CV mode. (a) $R_B = 50\,\Omega$ and (b) $R_B = 100\,\Omega$.

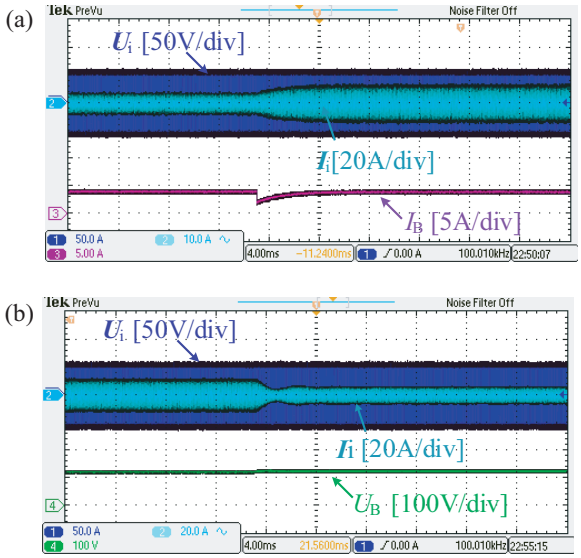

FIGURE 11. Transient waveforms when RB suddenly changes (a) from $5\,\Omega$ to $10\,\Omega$ in CC mode and (b) from $50\,\Omega$ to $100\,\Omega$ in CV mode.

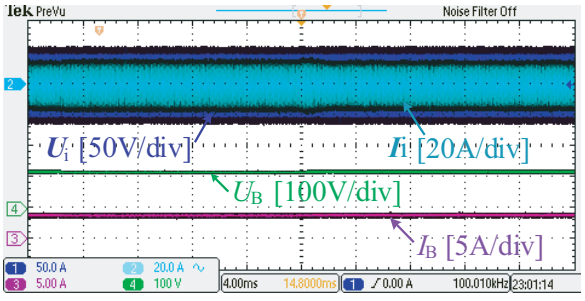

FIGURE 12. Experimental waveforms of switching process from CC to CV mode.

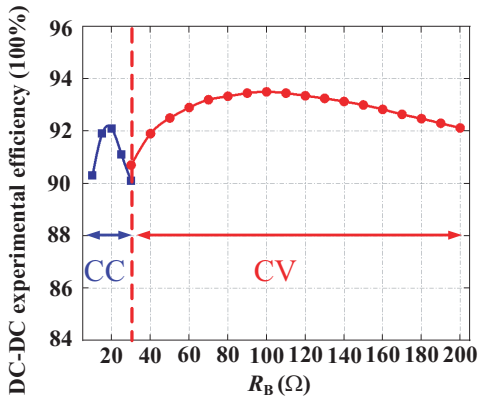

FIGURE 13. The DC-DC experimental efficiency of the proposed system.

CV mode do not fluctuate significantly, proving the reliability of the proposed system.

The switching process from CC to CV is experimentally tested, as shown in Fig. 12. As can be seen from Fig. 12, the system achieves a smooth transition from CC to CV mode, which verifies the stability of the proposed system.

The DC-DC experimental efficiency of the proposed system is shown in Fig. 13. From Fig. 13, the maximum efficiency points of the proposed system in CC mode and CV mode are 92.1% and 93.5%, respectively. In addition, the entire charging process maintains high efficiency.

4. CONCLUSION

By introducing an AC switch and a MOSFET into a traditional LCC-LCC structure, transition from CC mode to CV mode can be achieved by controlling the status of the AC switch and MOSFET Q_5. Compared with existing similar technical structures, this system introduces fewer switches and passive components, simplifying the circuit structure and saving costs. During the entire charging process, the system can implement ZPA operation and maintain high efficiency. Besides, it works at a fixed operating frequency to avoid frequency bifurcation and maintain the stability of the system. Finally, the feasibility of this system was verified by establishing an experimental prototype with a rated power of 480 W.

ACKNOWLEDGEMENT

This work was supported in part by Scientific Research Youth Foundation of Hunan Province Education Department of China (22B0803), in part by Employment and Education Foundation of The Second Phase of The Department of College Students of The Ministry of Education of China (20230106677), in part by Guiding Science and Technology Programme Foundation of Yongzhou City of China (2022-YZKJZD-010), in part by Natural Science Foundation of Hunan Province (NO. 2024JJ7186).

REFERENCES

[1] Xu, Y., Y. Li, Y. Chen, W. Zhou, R. Mai, and Z. He, "A multiple-gain-reconfigurable-rectifier-based ipt system for battery multi-stage constant current high-efficiency wireless charging," *IEEE Transactions on Power Electronics*, Vol. 39, No. 1, 1853–1869, Jan. 2024.

[2] Wang, H., Y. Wu, Z. Shen, W. Pan, X. Chen, and Y. Zhang, "High-misalignment-tolerant dual-channel inductive power transfer system based on cross-shaped reversed-winding-incorporated solenoid pad," *IEEE Transactions on Industrial Electronics*, 2024, doi: 10.1109/TIE.2024.3360620.

[3] Lin, H., C. Cai, J. Chen, Y. Gao, S. Vazquez, and Y. Li, "Modulation and control independent dead-zone compensation for H-bridge converters: A simplified digital logic scheme," *IEEE Transactions on Industrial Electronics*, 2024, doi: 10.1109/TIE.2024.3370975.

[4] Xiang, Y., H. S.-H. Chung, and H. Lin, "Light implementation scheme of ANN-based explicit model-predictive control for DC–DC power converters," *IEEE Transactions on Industrial Informatics*, Vol. 20, No. 3, 4065–4078, Mar. 2024.

[5] Li, S. and C. C. Mi, "Wireless power transfer for electric vehicle applications," *IEEE Journal of Emerging and Selected Topics in Power Electronics*, Vol. 3, No. 1, 4–17, Mar. 2015.

[6] Si, P., A. P. Hu, S. Malpas, and D. Budgett, "A frequency control method for regulating wireless power to implantable devices," *IEEE Transactions on Biomedical Circuits and Systems*, Vol. 2, No. 1, 22–29, Mar. 2008.

[7] Chen, Q., S. C. Wong, C. K. Tse, and X. Ruan, "Analysis, design, and control of a transcutaneous power regulator for artificial hearts," *IEEE Transactions on Biomedical Circuits and Systems*, Vol. 3, No. 1, 23–31, 2009.

[8] Jayalath, S. and A. Khan, "Design, challenges, and trends of inductive power transfer couplers for electric vehicles: A review," *IEEE Journal of Emerging and Selected Topics in Power Electronics*, Vol. 9, No. 5, 6196–6218, Oct. 2021.

[9] Li, W., H. Zhao, S. Li, J. Deng, T. Kan, and C. C. Mi, "Integrated LCC compensation topology for wireless charger in electric and plug-in electric vehicles," *IEEE Transactions on Industrial Electronics*, Vol. 62, No. 7, 4215–4225, Jul. 2015.

[10] Zhang, P., M. Saeedifard, O. C. Onar, Q. Yang, and C. Cai, "A field enhancement integration design featuring misalignment tolerance for wireless EV charging using LCL topology," *IEEE Transactions on Power Electronics*, Vol. 36, No. 4, 3852–3867, Apr. 2021.

[11] Chen, Z., X. Zhang, F. Xu, M. Li, Z. Yuan, and Q. Yang, "Wide rotation-misalignment-tolerance design of magnetic coupled structure for AUVs wireless charging system," *IEEE Transactions on Industrial Electronics*, 2024, doi: 10.1109/TIE.2024.3382978.

[12] Wang, X., M. Leng, X. Zhang, Q. Tian, X. Zhou, B. Guo, and H. Ma, "Multioutput wireless charger for drone swarms with reduced switch requirements and independent regulation capability," *IEEE Transactions on Industrial Electronics*, Vol. 71, No. 5, 4883–4895, May 2024.

[13] Zeng, Y., C. Lu, R. Liu, X. He, C. Rong, and M. Liu, "Wireless power and data transfer system using multidirectional magnetic coupler for swarm AUVs," *IEEE Transactions on Power Electronics*, Vol. 38, No. 2, 1440–1444, Feb. 2023.

[14] Zeng, Y., C. Rong, C. Lu, X. Tao, X. Liu, R. Liu, and M. Liu, "Misalignment insensitive wireless power transfer system using a hybrid transmitter for autonomous underwater vehicles," *IEEE Transactions on Industry Applications*, Vol. 58, No. 1, 1298–1306, Jan.-Feb. 2022.

[15] Xu, Y., R. Mai, W. Liu, S. Pan, Y. Chen, Z. He, Y. Li, and U. K. Madawala, "A switchable-LCL-circuit-based IPT system with high efficiency for reefer containers," *IEEE Transactions on Power Electronics*, Vol. 36, No. 2, 1253–1258, Feb. 2021.

[16] Wang, Y., H. Liu, H. Yu, P. Wheeler, Q. Zhou, and S. Zhao, "A hybrid battery wireless charger for self-adapting battery charging curve and anti-misalignment," *IEEE Journal of Emerging and Selected Topics in Industrial Electronics*, Vol. 4, No. 4, 1192–1203, Oct. 2023.

[17] Berger, A., M. Agostinelli, S. Vesti, J. A. Oliver, J. A. Cobos, and M. Huemer, "A wireless charging system applying phase-shift and amplitude control to maximize efficiency and extractable power," *IEEE Transactions on Power Electronics*, Vol. 30, No. 11, 6338–6348, Nov. 2015.

[18] Colak, K., E. Asa, M. Bojarski, D. Czarkowski, and O. C. Onar, "A novel phase-shift control of semibridgeless active rectifier for wireless power transfer," *IEEE Transactions on Power Electronics*, Vol. 30, No. 11, 6288–6297, Nov. 2015.

[19] Liu, N. and T. G. Habetler, "Design of a universal inductive charger for multiple electric vehicle models," *IEEE Transactions on Power Electronics*, Vol. 30, No. 11, 6378–6390, Nov. 2015.

[20] Gati, E., G. Kampitsis, and S. Manias, "Variable frequency controller for inductive power transfer in dynamic conditions," *IEEE Transactions on Power Electronics*, Vol. 32, No. 2, 1684–1696, Feb. 2017.

[21] Li, Z., C. Zhu, J. Jiang, K. Song, and G. Wei, "A 3-kW wireless power transfer system for sightseeing car supercapacitor charge," *IEEE Transactions on Power Electronics*, Vol. 32, No. 5, 3301–3316, May 2017.

[22] Wu, H. H., A. Gilchrist, K. D. Sealy, and D. Bronson, "A high efficiency 5 kW inductive charger for EVs using dual side control," *IEEE Transactions on Industrial Informatics*, Vol. 8, No. 3, 585–595, Aug. 2012.

[23] Chen, Y., B. Yang, Z. Kou, Z. He, G. Cao, and R. Mai, "Hybrid and reconfigurable IPT systems with high-misalignment tolerance for constant-current and constant-voltage battery charging," *IEEE Transactions on Power Electronics*, Vol. 33, No. 10, 8259–8269, Oct. 2018.

[24] Li, Y., J. Hu, M. Liu, Y. Chen, K. W. Chan, Z. He, and R. Mai, "Reconfigurable intermediate resonant circuit based WPT system with load-independent constant output current and voltage for charging battery," *IEEE Transactions on Power Electronics*, Vol. 34, No. 3, 1988–1992, Mar. 2019.

[25] Chen, Y., M. Li, B. Yang, S. Chen, Q. Li, Z. He, and R. Mai, "Variable-parameter T-circuit-based IPT system charging battery with constant current or constant voltage output," *IEEE Transactions on Power Electronics*, Vol. 35, No. 2, 1672–1684, Feb. 2020.

[26] Mai, R., Y. Chen, Y. Zhang, N. Yang, G. Cao, and Z. He, "Optimization of the passive components for an S-LCC topology-based WPT system for charging massive electric bicycles," *IEEE Transactions on Industrial Electronics*, Vol. 65, No. 7, 5497–5508, Jul. 2018.

[27] Yang, L., X. Li, S. Liu, Z. Xu, and C. Cai, "Analysis and design of an LCCC/S-compensated WPT system with constant output characteristics for battery charging applications," *IEEE Journal of Emerging and Selected Topics in Power Electronics*, Vol. 9, No. 1, 1169–1180, Feb. 2021.

[28] Vu, V.-B., D.-H. Tran, and W. Choi, "Implementation of the constant current and constant voltage charge of inductive power transfer systems with the double-sided lcc compensation topology for electric vehicle battery charge applications," *IEEE Transactions on Power Electronics*, Vol. 33, No. 9, 7398–7410, Sep. 2018.

[29] Lu, J., G. Zhu, D. Lin, Y. Zhang, J. Jiang, and C. C. Mi, "Unified load-independent ZPA analysis and design in CC and CV modes of higher order resonant circuits for WPT systems," *IEEE Transactions on Transportation Electrification*, Vol. 5, No. 4, 977–987, Dec. 2019.

[30] Yang, L., L. Ren, Y. Shi, M. Wang, and Z. Geng, "Analysis and design of a S/S/P-compensated three-coil structure WPT system with constant current and constant voltage output," *IEEE Journal of Emerging and Selected Topics in Power Electronics*, Vol. 11, No. 3, 2487–2500, Jun. 2023.